X-RAY SURFACE SCATTERING STUDIES OF MOLECULAR ORDERING AT LIQUID-LIQUID INTERFACES

MARK L. SCHLOSSMAN, MING LI, DRAGOSLAV M. MITRINOVIC, ALEKSEY M. TIKHONOV
Department of Physics, University of Illinois, Chicago, IL 60607, schloss@uic.edu

ABSTRACT

We present our recent progress in using synchrotron x-ray surface scattering techniques to study several different aspects of ordering at liquid-liquid interfaces. (1) We present measurements of the interfacial width at the water-alkane interface for a series of different chain length alkanes. The width for the shortest chain length studied is in agreement with capillary wave theory. However, significant deviations occur for longer chain lengths, indicating the presence of molecular ordering at the interface. (2) Under appropriate conditions, a surfactant monolayer forms at the interface between water and a hexane solution of a fluorinated surfactant. Reflectivity measurements that probe the electron density profile normal to the interface provide information about the surfactant ordering. This monolayer undergoes a solid to gas transition as a function of temperature. Diffuse scattering near the transition reveals the presence of islands. (3) Equilibrium interfaces between two aqueous phases containing PEG (polyethylene glycol) and potassium phosphate salts can be studied. We present studies of coherent capillary wave fluctuations between two interfaces of a thin film of this biphase system. We also demonstrate that biological macromolecules can be trapped and studied at this aqueous-aqueous interface.

INTRODUCTION

An outstanding problem in the area of interfacial phenomena is the determination of structure at liquid-liquid interfaces. These interfaces play an important role in many chemical and biological systems in addition to being interesting model systems for study of the statistical physics of interfaces and membranes. Surfactant molecules naturally arrange themselves at liquid interfaces and, in the case of aqueous-organic interfaces, bring together materials on the microscopic scale that may be otherwise immiscible. Biological membranes which exist at aqueous-aqueous interfaces play a critically important role in many cell processes. In spite of their importance, there remain fundamental questions in the study of liquid-liquid interfaces that have been barely addressed. There is currently a poor understanding of electron and molecular density profiles both normal to the interface and within the interface.

Few experimental techniques are capable of directly probing the molecular order or condensed matter states at a single liquid-liquid interface, non-linear optical studies being a recently developed, notable exception that provides information about molecular conformations [1-3]. Recently, x-ray and neutron surface scattering have been applied to the study of liquid-liquid interfaces [4-8]. Here, we discuss briefly several investigations that probe fundamental aspects of molecular ordering at liquid-liquid interfaces. In addition, we also discuss a system of potential use for probing biological processes at aqueous-aqueous interfaces.

EXPERIMENTS AND DISCUSSION

Experimental Methods

These x-ray surface scattering measurements were conducted at beamline X19C at the National Synchrotron Light Source (Brookhaven National Laboratory, USA) with a liquid surface spectrometer and measurement techniques described in detail elsewhere [9]. For x-ray reflectivity, the incident angle α is equal to the scattered angle β (see Fig. 1). The reflected x-ray intensity is normalized to the incident intensity and measured as a function of the wave vector transfer normal to the plane of the interface, $Q_z = (4\pi/\lambda)\sin(\alpha)$, where $\lambda = 0.0825 \pm 0.0002$ nm is the x-ray wavelength for these measurements. For off-specular diffuse scattering the incident and scattered angles are different.

Mat. Res. Soc. Symp. Proc. Vol. 590 © 2000 Materials Research Society

For measurements at the water-alkane interface, the liquids were contained in vapor-tight, temperature-controlled, polycarbonate or stainless steel sample cells with mylar x-ray windows. The sample cells had x-ray path lengths through the upper phase of either 25, 50, or 76 mm. The liquids were first stirred and allowed to reach thermal equilibrium. To reduce most of the curvature from the meniscus formed at the cell windows, the windows are angled 25° from the vertical (see Fig. 1). However, fine tuning of the interfacial flatness is required. This is accomplished by pinning the meniscus to the cell windows (by roughening the windows), then rotating the entire sample. This twists the interface to yield a very flat region suitable for x-ray scattering. Alternatively, the liquid volume can be adjusted to flatten the interface.

Measurements at the aqueous-aqueous interface were from liquids placed in a circular teflon trough of diameter 75 mm. This trough was in a temperature controlled, closed container.

High purity water was produced from a Barnstead NanoPure system. High purity alkanes were purchased and then further purified by filtration through basic alumina. Their purity was confirmed by interfacial tension measurements. Other chemicals were used as received from the manufacturer.

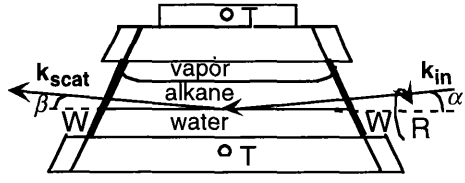

Fig. 1 Cross-sectional view of sample cell for water-alkane measurements; W - mylar windows; T - thermistor to measure temperature; R - rotation about the horizontal used to fine tune the sample flatness. The kinematics of surface x-ray reflectivity is also indicated: $\mathbf{k}_{in}$ is the incoming x-ray wave vector, $\mathbf{k}_{scat}$ is the scattered wave vector, α is the angle of incidence and reflection.

Water-Alkane Interfaces

Of fundamental importance in the study of liquid-liquid interfaces is the interface between two pure liquids such as water and alkane. This can be used as a model system to understand the interactions of alkyl chains with aqueous phases. A number of molecular dynamics simulations have focused upon the issues of the interfacial width and orientational order close to the interface. Molecular dynamics simulations by Buuren et al. found that the interfacial width depends sensitively upon the intermolecular potentials [10]. Here, we show that x-ray reflectivity can be used to measure the interfacial width between water and a series of alkanes.

X-ray reflectivity measurements as a function of the reflection angle from a bulk interface can be analyzed to yield an electron density profile along the normal to the interface (and averaged over the plane of the interface) with a resolution of a fraction of a nanometer [11]. Figure 2 illustrates the x-ray reflectivity, $R(Q_z)$, measured from the water-hexane interface at 32.00 °C [7]. The reflectivity varies with the angle of reflection, α, expressed here in terms of the wave vector transfer normal to the interface, $Q_z = (4\pi/\lambda)\sin\alpha$. Also shown is the Fresnel reflectivity, $R_F(Q_z)$, predicted for an ideal, smooth and flat interface. Both of these curves have a small region of constant reflectivity (equal to 1) below a critical wave vector transfer, $Q_c = 0.123$ nm^{-1}, corresponding to a region of total reflection. Both curves then drop off rapidly and smoothly with increasing wave vector transfer.

Although the qualitative features of the ideal and measured curves are similar, the reduction in intensity of the measured reflectivity at larger wave vector transfer is the result of x-rays being scattered by interfacial roughness due to thermally induced capillary wave fluctuations. The classical capillary wave model for the fluctuations [12] corresponds to an error function profile for the electron density averaged over the plane of the interface, $\langle\rho(z)\rangle$. For this interfacial profile the distorted wave Born approximation expresses the reflected intensity as [13],

$$R(Q_z) \cong \left|\frac{Q_z - Q_z^T}{Q_z + Q_z^T}\right|^2 \exp(-Q_z Q_z^T \sigma^2), \qquad (1)$$

where $Q_z^T \equiv \sqrt{Q_z^2 - Q_c^2}$ is the z-component of wave vector transfer with respect to the lower phase. A fit of the data to Eq.(1) using a single fitting parameter, σ, is illustrated by the solid line in Fig. 2 and yields the interfacial width $\sigma = 3.3 \pm 0.25$ Å.

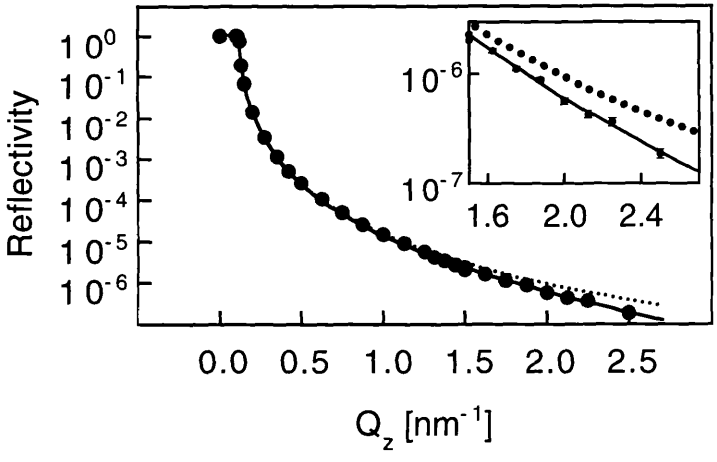

Fig. 2 X-ray reflectivity from the water-hexane interface as a function of wave vector transfer normal to the interface. ●, measurements at 32.00 °C; solid line through the soild circles, fit described in the text; dotted line, Fresnel reflectivity for ideal interface. The inset is an expanded view of the high Q_z region. Error bars on the data are similar to the symbol size in the inset.

In addition to the capillary wave contribution just discussed the interfacial width may also contain a contribution from an intrinsic profile described, for example, by van der Waals theories [14]. In the spirit of a hybrid model of the interface that describes this intrinsic profile roughened by capillary waves, the total interfacial width, σ_{total}, can be represented as a combination of an intrinsic profile width, σ_o, and the capillary wave contribution [15-17],

$$\sigma_{total}^2 = \sigma_o^2 + \frac{k_B T}{2\pi\gamma} \int_{q_{\min}}^{q_{\max}} \frac{q\,dq}{q^2 + \xi_{\|}^{-2}} \equiv \sigma_o^2 + \sigma_{cap}^2, \qquad (2)$$

where $k_B T$ is Boltzmann's constant times the temperature, γ is the interfacial tension, the correlation length, $\xi_{\|}$, is given by $\xi_{\|}^2 = \gamma / \Delta\rho_m g$ and determines the exponential decay of the interfacial correlations given by the height-height correlation function of interfacial motion [18], $\Delta\rho_m$ is the mass density difference of the two phases, and g is the gravitational acceleration. The wave vector, q, represents the in-plane capillary waves. The limit $q_{\min}$ is determined by the instrumental resolution that sets the largest in-plane capillary wavelength that the measurement probes. The limit, $q_{\max}$, is determined by the cutoff for the smallest wavelength capillary waves that the interface can support. Direct calculation of σ_{cap} using the literature value of the interfacial

tension (51.4 mN/m at $T = 22$ °C) [19] and $q_{max} = 2\pi/0.5$ nm^{-1} yields $\sigma_{cap} = 3.29$ Å, in agreement with our measurement of $\sigma = 3.3$ Å. This indicates that the intrinsic profile width, σ_o, is small for this interface, $\sigma_o < 1.5$Å.

We have extended these measurements to interfaces between water and longer chain alkanes. The x-ray reflectivity is similar in form to the measurements in Fig. 2 and can be fit well with the expression in Eq. (1). The results for the interfacial width squared, σ^2, are shown in Fig. 3. For alkanes longer than hexane there is a significant deviation of the measured interfacial width from the prediction of capillary wave theory. This indicates the presence of molecular ordering at the interface that can be characterized by an intrinsic profile width, σ_o, as in Eq. (2). Although it may have been expected that additional interfacial ordering would be monotonic as a function of chain length (as illustrated by the solid line in Fig. 3), our measurements indicate a statistically significant deviation from monotonicity.

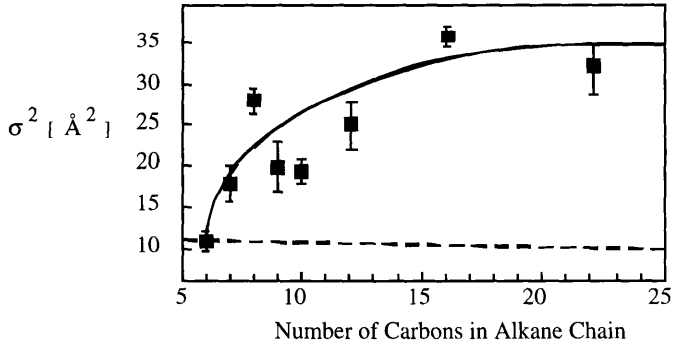

Fig. 3 Interfacial width (squared) determined by fitting x-ray reflectivity measurements from the water-alkane interface as a function of alkane carbon number. The dashed line indicates, approximately, the prediction for the interfacial width from capillary wave theory. The solid line is drawn as a guide to the eye.

Soluble Fluorinated Surfactants at the Water-Hexane Interface

The few available thermodynamic or spectroscopic measurements indicate that soluble and insoluble amphiphilic monolayers at water-oil interfaces are more loosely packed than the corresponding monolayers at the water-vapor interface [20-22]. In particular, the aliphatic tail groups of the amphiphiles exhibit greater chain disorder, possibly because the oil phase acts as a solvent for the chains at the interface [22]. Therefore, the chains are further from their neighbors than in a close packed solid. This reduces the van der Waals attractive forces between the alkyl chains, but allows for a higher conformational entropy of these flexible chains. Monolayers formed from surfactants soluble in the oil phase are expected to be disordered and in a liquid or gas phase at liquid-liquid interfaces [22].

To explore the ordering in a monolayer of soluble surfactants at the liquid-liquid interface we studied monolayers of $F(CF_2)_{10}(CH_2)_2OH$ (denoted here as $FC_{12}OH$) self-assembled from a solution ($2x10^{-3}$ mol/kg) in hexane onto the solution-water interface [23, 24]. Figure 4 illustrates x-ray reflectivity measurements at T=32.00 (±0.03)°C from the monolayer at the water–(hexane solution) interface [8]. Also shown are measurements from the pure water-hexane interface at the same temperature and measurements from the water-(hexane solution) interface at T=48.00°C. These curves have a small region of constant reflectivity (nearly equal to 1) below a critical wave vector transfer, $Q_c = 0.0123$ Å^{-1}, corresponding to a region of total reflection. The enhanced reflectivity at higher Q_z from the water–(hexane solution) interface at T=32.00°C is due to a constructive interference of x-rays reflected from the top of the fluorinated monolayer with x-rays

reflected from the bottom of the monolayer (inset, Fig. 4). The reflectivity from the water-(hexane solution) interface at T=48.00 °C is nearly identical to the measurements from the pure water-hexane interface and indicates that most of the $FC_{12}OH$ molecules have desorbed from the interface at this temperature.

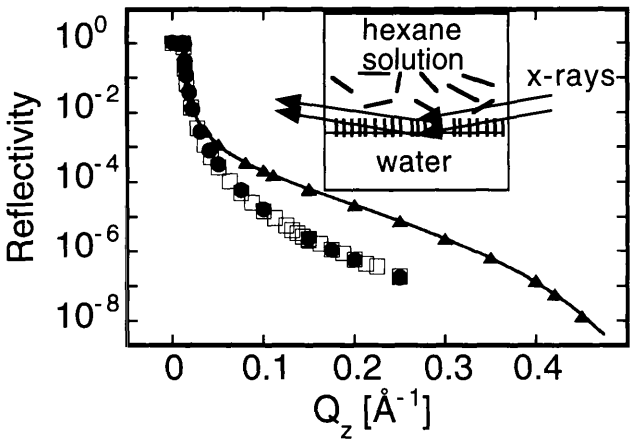

Fig. 4 X-ray reflectivity from the water–(hexane solution of $F(CF_2)_{10}(CH_2)_2OH$) interface at T=32°C, triangles; T=48°C, solid circles; pure water-hexane interface at T=32°C, open squares. Inset is a cartoon of the solid surfactant monolayer that forms at T=32°C.

These data can be analyzed by using a general expression, derived from the first Born approximation for x-ray scattering, that relates the reflectivity to the electron density gradient normal to the interface, $d\langle\rho(z)\rangle/dz$ (averaged over the interfacial plane), and written as [11]

$$\frac{R(Q_z)}{R_F(Q_z)} \cong \left| \frac{1}{\Delta\rho_{bulk}} \int dz \frac{d\langle\rho(z)\rangle}{dz} \exp(iQ_z z) \right|^2 , \qquad (3)$$

where $\Delta\rho_{e,bulk} = \rho_{e,bulk,lower} - \rho_{e,bulk,upper}$ and $R_F(Q_z)$ is the Fresnel reflectivity predicted for an ideal, smooth and flat interface [25]. The layer of $FC_{12}OH$ is modeled simply as a thin slab of higher electron density sandwiched between two bulk liquids. The interfaces of the top and bottom of this slab are roughened by thermal capillary waves, characterized by the roughness parameter, σ. The reflectivity calculated from Eq.(3) using the slab model for the electron density is fit to the data to yield values for the three fitting parameters: the slab thickness $L = 1.24 \pm 0.03$ nm, $\sigma = 0.36 \pm 0.02$ nm, and the slab electron density $\rho_f = 1.90 \pm 0.04$ (see Fig. 4) [8].

Our measurement of the electron density of the monolayer at T=32.00°C, $\rho_f = 1.90 \pm 0.04$, corresponds to a mass density of 2.19 ± 0.05 g/cm^3. This agrees with the density of bulk solid fluoroalkane phases (e.g., for n-$C_{20}F_{42}$) which have a density of either 2.23 g/cm^3 for the monoclinic crystal phase or 2.16 g/cm^3 for the rhombohedral rotator solid phase [26]. The error bars on our measurement of ρ_f do not allow us to distinguish between these two different solid phases. However, these measurements exclude the possibility that the $FC_{12}OH$ monolayer at the water-hexane interface is in a liquid monolayer phase (bulk liquid fluoroalkanes have a mass density of approximately 1.7 g/cm^3) [26, 27].

A similar analysis of the data from the water–(hexane solution) interface at T=48.00°C indicates that a conservative upper limit to the surface coverage of $FC_{12}OH$ is approximately 1.5% [8]. The transition from the solid $FC_{12}OH$ monolayer to this gaseous monolayer at higher temperature can be studied by measuring reflectivity as a function of temperature. Figure 5 indicates the first heating-cooling cycle through this transition.

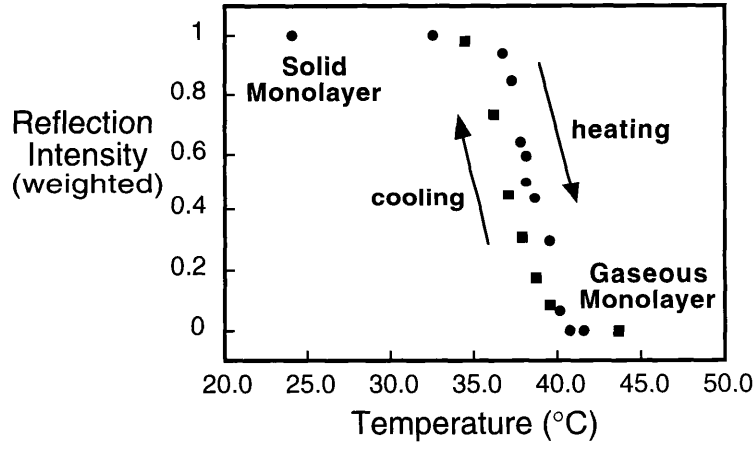

Fig. 5 Reflection intensity at $Q_z = 0.1$ Å^{-1} weighted so that a value of 1 indicates the presence of the solid monolayer phase while the value of 0 indicates the gaseous monolayer. This temperature scan reveals hysteresis through the solid–gas monolayer transition of $F(CF_2)_{10}(CH_2)_2OH$ at the water–(hexane solution) interface.

We believe that the transition region represents an interface with coexisting solid and gas monolayer phases. This is consistent with enhanced off-specular diffuse scattering that we measured in this transition region. Off-specular diffuse scattering for the heating cycle is illustrated in Fig. 6. This scattering can be described by the distorted wave Born approximation as,

$$I(\mathbf{Q}) \propto |T(\alpha)|^2 \, |T(\beta)|^2 \, |F(\mathbf{Q})|^2 \, |S(\mathbf{Q})|^2 \qquad (4)$$

where α is the incident angle; β is the scattering angle; the wave vector transfer, $\mathbf{Q} = \mathbf{k}_{scat} - \mathbf{k}_{in}$, is the difference between the incoming and scattered wave vectors; $F(\mathbf{Q})$ is the form factor for a particle; $S(\mathbf{Q})$ is the structure factor for the assembly of particles; $T(\alpha)$ or $T(\beta)$ are the Fresnel transmission coefficients [28, 29]. The tall, narrow peaks in the center of the scans in Fig. 6 occur when the incident angle, α, is equal to the scattering angle, β, and correspond to the specular reflectivity. In Fig. 6 a small peak appears at small β when $\beta = \theta_c$ (the angle for total reflection) and is known as a surface enhancement or Yoneda peak [30, 31].

Here, we are interested in the excess diffuse scattering in the "shoulders" immediately adjacent to the tall specular peaks in Fig. 6. The shape of this scattering is determined primarily by the form and structure factors. The shoulders in the measurement at 39.6°C illustrate essentially the shape of the form factor and reveal the presence of islands (or disks) of the solid phase on the order of a few micrometers in diameter. The sequence of lower temperatures (39.1°C, 38.9°C, and 38.3°C) indicate the presence of additional diffuse scattering due to the assembly of islands. The small peaks that appear in the shoulders of the specular peak indicate that the islands are spatially correlated. As the system is heated from 38.3°C to 39.6°C these small

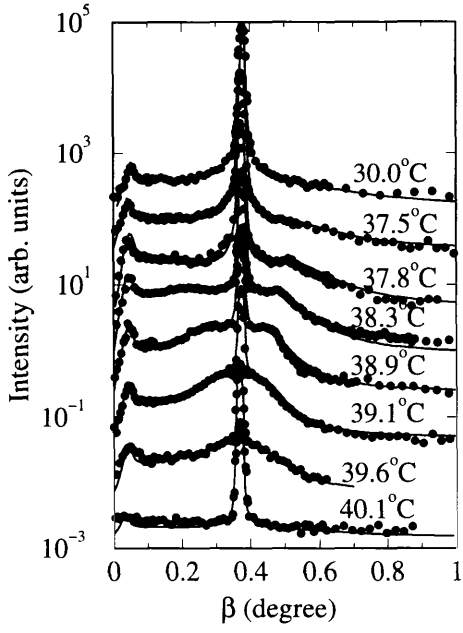

Fig. 6 Off-specular diffuse scattering for temperatures scanned through the range of the solid to gas monolayer transition of $F(CF_2)_{10}(CH_2)_2OH$ at the water–(hexane solution) interface. At 30°C the monolayer is in the low temperature solid phase; at 40.1°C it is in the high temperature gas phase. Additional diffuse scattering in the range $37.5°C < T < 40.1°C$ indicates the presence of islands of the solid phase. The curves are offset for clarity.

peaks move closer to the specular. This shows that the islands are spaced progressively further apart as the monolayer undergoes a transition from a solid to a gas phase. Over a narrow range in temperature of less than 0.15 °C (not shown in Fig. 6) the islands disappear.

An important feature of studies of the liquid-liquid interface is the ability to characterize the role of the upper phase on the structural order within, for example, monolayers at the interface. To gain some insight into the role of the upper-phase hexane on the ordering of the low temperature $FC_{12}OH$ solid phase monolayers, we studied a similar transition in $FC_{12}OH$ monolayers supported on the water-vapor interface. The $FC_{12}OH$ monolayer was spread in the crystalline island phase at an inverse density of 0.4 nm^2/molecule. Since the crystalline unit cell size is 0.29 nm^2/molecule there is excess area at the interface that allows the monolayer to undergo a transition to a liquid or gaseous disordered phase. X-ray grazing incidence diffraction measurements indicate that an order to disorder phase transition occurs between 58.8 °C and 62.09 °C, slightly more than 20 °C higher than the solid-gas transition in the $FC_{12}OH$ monolayer at the water–(hexane solution) interface. Therefore, the presence of the hexane solvent acts to disorder the monolayer at a lower temperature.

Aqueous-Aqueous Interfaces [32]

One of the most tantalizing areas for investigation of liquid-liquid interfaces is biological phenomena. Although biological membranes exist at liquid-liquid interfaces, it has not been possible previously to study molecular ordering and structure on the sub-nanometer scale within a membrane at the liquid-liquid interface. Biological membranes are complex bilayer structures of lipids and proteins. They separate the inside and outside of cells as well as the inside and outside of intracellular organelles within cells. These membranes exist at aqueous-aqueous interfaces and play a critical role in mediating biological communication between cells and transport of material into and out of the cell.

Although we have successfully applied x-ray reflectivity and diffuse scattering to the study of the liquid-liquid interface, we have not been able to use x-ray grazing incidence diffraction because of the large absorption and background scattering from the upper liquid phase. This diffraction technique allows the in-plane order at an interface to be probed and is likely to be very important in the study of biological structures. Therefore, we chose to develop an aqueous-aqueous interface where the upper phase is a thin film. This was also necessary because of the much larger x-ray absorption that would occur in an upper aqueous phase as compared to the upper alkane phases previously discussed.

Aqueous solutions of polymers and salts are well known to separate into two equilibrium phases. We chose to use biologically compatible polymer and salts, polyethylene glycol (PEG), and potassium phosphates. Once mixed in the proper proportions the resulting solution phase separates into a PEG-rich phase (the lighter, upper phase) and a salt-rich phase. Under the appropriate conditions the PEG-rich phase does not completely wet the salt-rich phase. We extracted the lower, salt-rich phase, and placed a small drop of the PEG-rich phase on its surface. This PEG-rich phase then forms a microscopically thin film (due to partial wetting of the interface) in equilibrium with a reservoir consisting of the remainder of the small drop (see Fig. 7).

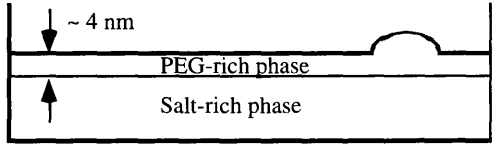

Fig. 7 Cartoon of a thin film of a PEG-rich phase in equilibrium with a PEG-rich reservoir drop and a bulk salt-rich phase.

Figure 8 shows the x-ray reflectivity (normalized to the Fresnel reflectivity) from this thin film system consisting of PEG (3400MW):K_2HPO_4:H_2O (13.2:28.9:57.9 wt %) at 35°C. The oscillations indicate the presence of the thin film of PEG-rich phase. The solid line in Fig. 8 is the result of a single slab model analysis of the data using Eq. (3). The analysis reveals that the film is 42 Å thick with an interfacial width between the PEG-rich phase and the vapor of $\sigma_{PEG\text{-}vapor}$ = 3.2 Å and an interfacial width between the salt-rich and PEG-rich phases of $\sigma_{salt\text{-}PEG}$ = 8.3 Å.

A combination of long and short-range forces is responsible for determining the equilibrium thickness of the thin PEG-rich film. As discussed in the wetting literature, the effect of these forces can be summarized in an interface potential that represents the potential energy between the PEG-vapor and salt-PEG interfaces as a function of the thickness of the film. Both of these interfaces fluctuate with capillary waves. If the fluctuations are conformal (in-phase, see Fig. 9a) then the equilibrium thickness is maintained locally throughout the film. If the fluctuations are non-conformal (or out of phase, see Fig. 9b) then the film thickness varies from point to point throughout the film. From the viewpoint of a local free energy, these variations in thickness will require a free energy penalty. In this local viewpoint we can determine the free energy cost to lowest order by expanding about the minimum of the interface potential. This results in a local

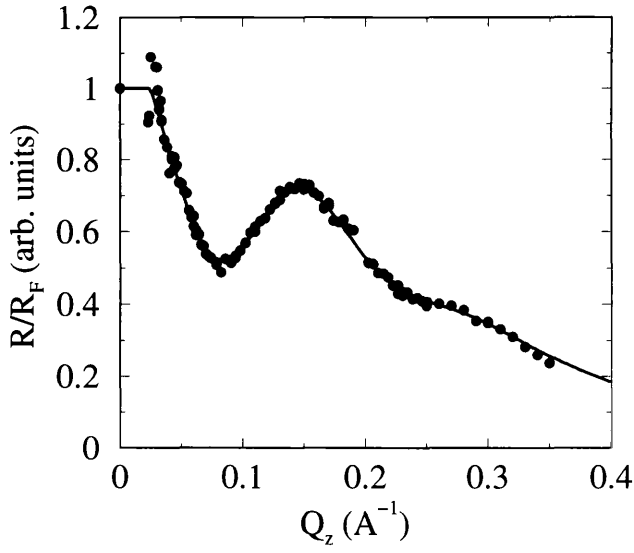

Fig. 8 X-ray reflectivity from a thin partially wet film of a PEG-rich phase on top of a salt-rich subphase. The solid line is a fit described in the text.

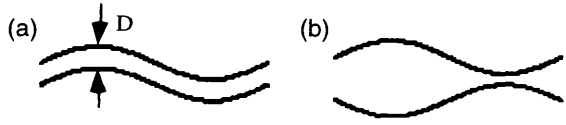

Fig. 9 (a) Conformal fluctuations of two interfaces that maintain the local equilibrium film thickness D throughout the entire film. (b) Non-conformal (out of phase) fluctuations in which the film thickness varies throughout the film.

modification of the capillary wave Hamiltonian expressed as

$$H = \int_{q\min}^{q\max} d^2s \left\{ \sum_{i=1,2} \left[\frac{1}{2}\gamma_i \left(|\nabla\zeta_i|^2 + \left(\frac{\zeta_i}{\xi_{ll,cw}} \right)^2 \right) \right] + B(\zeta_1 - \zeta_2)^2 \right\}, \qquad (5)$$

where i labels the two interfaces, $\zeta_i(x,y)$ represents the local height of each interface above a reference plane whose coordinates are $s = (x,y)$, and B represents the curvature of the interfacial potential near its minimum (we have assumed that the lowest order term in the interface coupling is quadratic). The Hamiltonian in Eq. (5) without the coupling term is the standard capillary wave Hamiltonian for two independent interfaces [12, 18]. This modified Hamiltonian is still Gaussian and can be analyzed by standard statistical mechanical methods to yield the ensemble averages of the correlation functions between the amplitudes of the capillary waves in reciprocal space. These, in turn, are used to predict the structure factor for off-specular diffuse scattering from the coupled capillary wave fluctuations of the two interfaces.

The interfacial coupling manifests itself experimentally in two ways. In the first, scans in Q_z slightly tuned off the specular condition (nearly longitudinal diffuse scans or so-called background scans) show oscillations that mimic the oscillations in the specular reflectivity curve (not shown). In the second, the form of the off-specular diffuse scattering taken by scanning the exit angle, β, at fixed incident angle, α, will be modified by the interfacial coupling. These latter scans are shown in Fig. 10. The fits yield a coupling parameter of $B = 8.6 \times 10^{-6}$ dyn/cmÅ^2.

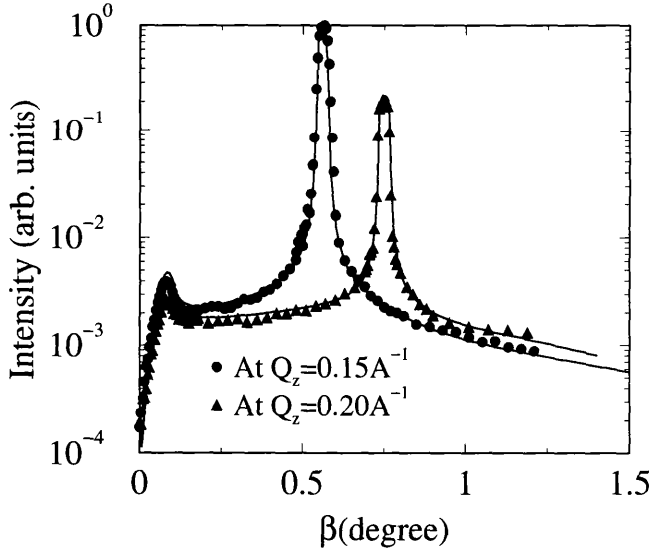

Fig. 10 Off-specular nearly transverse diffuse scattering from the capillary wave fluctuations of a thin PEG-rich film on top of a salt-rich subphase. The specular reflectivity for this thin film was shown in Fig. 8. The lines are fits to a model that contains coupled capillary wave fluctuations between the two interfaces.

To test the usefulness of this thin film system for the study of biological macromolecules or membranes the protein Ferritin (from horse spleen, purchased from Aldrich, 100 mg/ml ferritin in a NaCl 0.15 M solution) was adsorbed to the aqueous-aqueous interface between the thin PEG-rich film and the salt-rich subphase (see Fig. 11). To reduce the salt concentration to make the solution more favorable to the protein, we used a solution of PEG (8000MW):K_2HPO_4: KH_2PO_4:H_2O (5:9:6:80 wt %) at 32°C. Analysis of the x-ray reflectivity data from the thin film without the protein (shown in the bottom of Fig. 12) reveals that the film is 51 Å thick with an interfacial width between the PEG-rich phase and the vapor of $\sigma_{PEG\text{-}vapor}$ = 3.2 Å and an

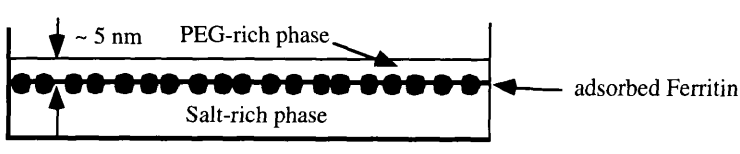

Fig. 11 Cartoon of adsorbed protein Ferritin at aqueous-aqueous interface.

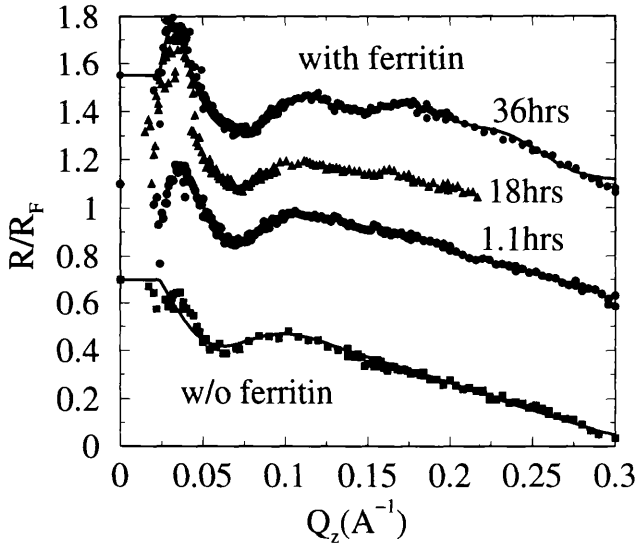

Fig. 12 X-ray reflectivity measurements show the evolution in time of the ferritin layer at the liquid-liquid interface. The lowest curve is the reflectivity before the ferritin is added. The solid line in the upper curve is a fit to a model of ferritin sandwiched between the PEG-rich and salt-rich phases. The curves are offset for clarity.

interfacial width between the salt-rich and PEG-rich phases of $\sigma_{salt\text{-}PEG}$ = 15.9 Å. The protein is added to the interface by injecting 0.8 µl of a ferritin solution into the salt-rich subphase (the solution was prepared by taking 20 µl of the as purchased ferritin in NaCl and diluting that in 5 ml of a 16 wt% PEG solution). Immediately after adding the protein solution a new peak is present in the reflectivity that indicates additional electron density at the interface (Fig. 12). Adsorption of ferritin at the interface continues until, after 36 hours, a well developed structure is present in the reflectivity. Our slab model analysis is consistent with the adsorption of ferritin at the liquid-liquid interface.

CONCLUSION

We have used x-ray reflectivity and diffuse scattering to study the molecular ordering at a variety of liquid-liquid interfaces. We have addressed the fundamental issue of ordering at pure water-alkane interfaces and demonstrated significant deviations from the predictions of capillary wave theory. This indicates the presence of molecular ordering of the alkanes at the interface. These effects are also currently unexplained by molecular dynamics simulations. We have also addressed the problem of characterizing the order of an equilibrium surfactant monolayer at the water-hexane interface. X-ray reflectivity was used to determine the thickness and electron density of the monolayer. This revealed that the monolayer is a solid at room temperature and undergoes a transition to a gas phase at higher temperatures. Off-specular diffuse scattering revealed that the solid monolayer breaks up into islands of solid phase in coexistence with the gas phase. As the temperature is increased all the solid islands are converted into a gas phase.

We also demonstrated that microscopically thin films can be formed with equilibrium aqueous biphase solutions. The thickness of the films is on the order of 4 - 5 nm. Capillary waves on the top and bottom surfaces of these films are correlated. The lower phase of this film is

an aqueous-aqueous interface that may prove to be useful for the investigation of biological membranes and macromolecules. In our first study of this nature we investigated the adsorption of the protein ferritin to this interface.

ACKNOWLEDGMENTS

We acknowledge collaborations with Zhengqing Huang (Brookhaven National Laboratory) and David Chaiko (Argonne National Laboratory). MLS gratefully acknowledges support from the NSF Division of Materials Research, the Petroleum Research Foundation administered by the American Chemical Society, the Chemical Technology Division of Argonne National Laboratory, and the UIC Campus Research Board. The National Synchrotron Light Source at Brookhaven National Laboratory is supported by the Department of Energy.

REFERENCES

1. S.G. Grubb, M.W. Kim, T. Rasing and Y.R. Shen, Langmuir **4**, 452 (1988).
2. J.C. Conboy, J.L. Daschbach and G.L. Richmond, Appl. Phys. A **59**, 623 (1994).
3. R.R. Naujok, D.A. Higgins, D.G. Hanken and R.M. Corn, J. Chem. Soc., Faraday Trans. **91**, 1411 (1995).
4. L.T. Lee, D. Langevin and B. Farnoux, Phys. Rev. Lett. **67**, 2678 (1991).
5. J.S. Phipps, R.M. Richardson, T. Cosgrove and A. Eaglesham, Langmuir **9**, 3530 (1993).
6. B.R. McClain, et al., Phys. Rev. Lett. **72**, 246 (1994).
7. D.M. Mitrinovic, Z. Zhang, S.M. Williams, Z. Huang and M.L. Schlossman, J. Phys. Chem. **103**, 1779 (1999).
8. Z. Zhang, D.M. Mitrinovic, S.M. Williams, Z. Huang and M.L. Schlossman, J. Chem. Phys. **110**, 7421 (1999).
9. M.L. Schlossman, et al., Rev. Sci. Instrum. **68**, 4372 (1997).
10. A.R.v. Buuren, S.-J. Marrink and H.J.C. Berendsen, J. Phys. Chem. **97**, 9206 (1993).
11. P.S. Pershan, Far. Disc. Chem. Soc. **89**, 231 (1990).
12. F.P. Buff, R.A. Lovett and F.H. Stillinger, Phys. Rev. Lett. **15**, 621 (1965).
13. S.K. Sinha, E.B. Sirota, S. Garoff and H.B. Stanley, Phys. Rev. B **38**, 2297 (1988).
14. J.S. Rowlinson and B. Widom, *Molecular Theory of Capillarity* (Clarendon Press, Oxford, 1982).
15. J.D. Weeks, J. Chem. Phys. **67**, 3106 (1977).
16. A. Braslau, et al., Phys. Rev. Lett. **54**, 114 (1985).
17. M.L. Schlossman, in *Encyclopedia of Applied Physics* (ed. Trigg, G.L.) (VCH Publishers, New York, 1997) pp. 311-336.
18. M.P. Gelfand and M.E. Fisher, Physica A **166**, 1 (1990).
19. A. Goebel and K. Lunkenheimer, Langmuir **13**, 369 (1997).
20. B.Y. Yue, C.M. Jackson, J.A.G. Taylor, J. Mingins and B.A. Pethica, J. Chem. Soc. Faraday I **72**, 2685 (1976).
21. M.C. Messmer, J.C. Conboy and G.L. Richmond, J. Am. Chem. Soc. **117**, 8039 (1995).
22. G.L. Richmond, Analytical Chemistry **69**, 536A (1997).
23. Y. Hayami, A. Uemura, N. Ikeda, M. Aratono and K. Motomura, J. Coll. Int. Sci. **172**, 142 (1995).
24. T. Takiue, et al., J. Phys. Chem. **100**, 20122 (1996).
25. M. Born and E. Wolf, *Principles of Optics* (Pergamon Press, Oxford, 1980).
26. H. Schwickert, G. Strobl and M. Kimmig, J. Chem. Phys. **95**, 2800 (1991).
27. H.W. Starkweather, Macromolecules **19**, 1131 (1986).
28. R.S. Becker, J.A. Golovchenko and J.R. Patel, Phys. Rev. Lett. **50**, 153 (1983).
29. S. Dietrich and H. Wagner, Z. Phys. B **56**, 207 (1984).
30. Y. Yoneda, Phys. Rev. **131**, 2010 (1963).
31. M.L. Schlossman and P.S. Pershan, in *Light Scattering by Liquid Surfaces and Complementary Techniques* (ed. Langevin, D.) (Marcel Dekker Inc., New York, 1992) pp. 365-403.
32. In collaboration with David Chaiko (Argonne National Laboratory).